



**HAL**  
open science

## **AMMONIA BLENDED FUELS – ENERGY SOLUTIONS FOR A GREEN FUTURE**

S-E Zitouni, S Mashruk, N Mukundakumar, P Brequigny, A Zayoud, E Pucci, S Macchiavello, F Contino, Christine Mounaïm-Rousselle, R Bastiaans, et al.

► **To cite this version:**

S-E Zitouni, S Mashruk, N Mukundakumar, P Brequigny, A Zayoud, et al.. AMMONIA BLENDED FUELS – ENERGY SOLUTIONS FOR A GREEN FUTURE. 10th International Gas Turbine Conference, Oct 2021, virtual, Netherlands. hal-03519203

**HAL Id: hal-03519203**

**<https://hal.science/hal-03519203>**

Submitted on 10 Jan 2022

**HAL** is a multi-disciplinary open access archive for the deposit and dissemination of scientific research documents, whether they are published or not. The documents may come from teaching and research institutions in France or abroad, or from public or private research centers.

L'archive ouverte pluridisciplinaire **HAL**, est destinée au dépôt et à la diffusion de documents scientifiques de niveau recherche, publiés ou non, émanant des établissements d'enseignement et de recherche français ou étrangers, des laboratoires publics ou privés.

## AMMONIA BLENDED FUELS – ENERGY SOLUTIONS FOR A GREEN FUTURE

S-E. Zitouni\*<sup>1</sup>, S. Mashruk\*<sup>2</sup>, N. Mukundakumar<sup>3</sup>, P. Brequigny<sup>1</sup>, A. Zayoud<sup>4</sup>, E. Pucci<sup>5</sup>, S. Macchiavello<sup>6</sup>, F. Contino<sup>4</sup>, C. Mounaim-Rousselle<sup>1</sup>, R. Bastiaans<sup>3</sup>, A. Valera-Medina<sup>2</sup>

<sup>1</sup>Université d'Orléans, Laboratoire PRISME  
EA 4229, F45072 Orléans, France

<sup>2</sup>Cardiff University, College of Physical Sciences and Engineering  
Queen's Building, 14-17 The Parade, Cardiff CF24 3AA, United Kingdom

<sup>3</sup>Eindhoven University of Technology, Department of Mechanical Engineering  
PO Box 513, 5600 MB Eindhoven, Netherlands

<sup>4</sup>Université Catholique de Louvain, iMMC  
Place du Levant, 2 bte L5.04.03 B-1348, Louvain-la-Neuve, Belgium

<sup>5</sup>Baker Hughes, Nuovo Pignone Technologie  
Via F. Matteucci, 2 - 50127, Florence, Italy

<sup>6</sup>Rina Consulting S.p.A  
Via Cecchi, 6 - 16129, Genova, Italy

Corresponding Authors Email: <sup>(1)</sup> [seif-eddine.zitouni@univ-orleans.fr](mailto:seif-eddine.zitouni@univ-orleans.fr)  
<sup>(2)</sup> [MashrukS@cardiff.ac.uk](mailto:MashrukS@cardiff.ac.uk)

### ABSTRACT

Global warming is potentially the greatest challenge of this century, with anthropogenic CO<sub>2</sub> emissions the main source of greenhouse gas (GHGs) emissions. Recently, ammonia (NH<sub>3</sub>) has gained attention as a potential carbon-free energy vector (carrier). NH<sub>3</sub> can be produced from waste sources, renewable energy, coupled with already existing infrastructures for production and distribution. However, pure NH<sub>3</sub> suffers from low flame speed and potentially important nitrogen oxide (NO<sub>x</sub>) emissions. As such, blending fuels such as methane (CH<sub>4</sub>) or hydrogen (H<sub>2</sub>) with NH<sub>3</sub> could potentially address NH<sub>3</sub>'s poor combustion capacities.

Therefore, the program FLEXnCONFU has been conceived, supporting bespoke research to tackle some of the fundamental and applied challenges of using these blends. This paper addresses some of the current FLEXnCONFU's progress. Firstly, a series of experiments using a spherical expanding flame set-up was employed to

investigate potential increases in reactivity of NH<sub>3</sub> and its blends with H<sub>2</sub> and CH<sub>4</sub>. Secondly, direct numerical simulation (DNS) modelling of NH<sub>3</sub>/H<sub>2</sub> turbulent expanding spherical flames was performed at lean and rich conditions. Finally, this study also discusses experimental results from an industrial scale swirl burner with varying content of CH<sub>4</sub>/NH<sub>3</sub>/H<sub>2</sub> under rich condition ( $\Phi = 1.2$ ), in terms of radicals and exhaust emissions. The work is a step towards using non-conventional fuels such as NH<sub>3</sub> and H<sub>2</sub> and scaling up the technology from lab to industrial level.

### INTRODUCTION

Today's energy mix is heavily dominated by hydrocarbon fuels, with coal, crude oil and natural gas accounting for nearly three quarters of our global primary energy consumption (Ritchie and Roser (2020)). Fossil fuel combustion has well documented environmental impacts, with GHGs emissions responsible for climate change, potentially leading to ecological adversities; sea-level rise due to ice shrinkage around the poles, extreme weather

events and disrupted water systems, etc. (Letcher (2015)). One of the most harmful GHG augmenting atmospheric temperature is CO<sub>2</sub>, which alone contributes to nearly 30% of global warming effects (Chen, Fei and Wan (2019)). To attain zero-carbon emission targets, the deployment of carbon-free combustion systems has become pivotal to generate a balanced trajectory between human development, progress, and cohesion with the environment.

H<sub>2</sub> has been proposed as a credible fuel. Hydrogen's popularity stems from its advantageous zero CO<sub>2</sub> emission, while posing challenges for achieving a stable dry-low-NO<sub>x</sub>, to reach NO<sub>x</sub> emissions as low as those obtained by burning natural gas. Moreover, H<sub>2</sub> cannot be found naturally at industrial scales, with almost all current H<sub>2</sub> production supplied by fossil fuels, consuming 6% and 2% of global natural gas and coal production, respectively (I.E.A (2019)). Aside from the need to produce 'green' H<sub>2</sub> (through for example renewable based electrolysis), there remains major hurdles with respect to H<sub>2</sub> deployment, with the issue of reliable, economical and efficient storage and distribution infrastructure, coupled with the need to develop novel compression/liquefaction technologies as well as safety issues relating to leak detection among others (Pivovarov (2016)).

On the other hand, NH<sub>3</sub> can be considered an efficient H<sub>2</sub> carrier. The H<sub>2</sub> content of NH<sub>3</sub> is ~17.7% (higher than that, for example, ethanol, methanol or gasoline). Liquid NH<sub>3</sub> has a higher volumetric energy density than that of liquid H<sub>2</sub> (Service (2018)). Large scale NH<sub>3</sub> has been produced commercially on a world-wide scale for over a century, and as such, considerable amounts of infrastructures are already in place for storage and distribution. Storage requirements for NH<sub>3</sub> are comparable to those of propane, with storage pressure of H<sub>2</sub> approximately 90 times higher than that of NH<sub>3</sub> (700 vs 8 Bar), mainly owing to NH<sub>3</sub> much higher liquefaction temperature (298.8 K vs 20K). Furthermore, the shipping industry, which transports over 80% of worldwide NH<sub>3</sub> production, has already implemented safe industrial practices, mitigating the need for extensive NH<sub>3</sub> related safety preparations (Chai *et al.* (2021)).

Although NH<sub>3</sub> usage offers several advantages, NH<sub>3</sub> exhibits slow burning velocities (S<sub>L</sub>) often associated to low burning efficiency in engines. Furthermore, although a carbon free fuel, NH<sub>3</sub> combustion high fuel nitrogen oxides (NO<sub>x</sub>) emissions result in detrimental environmental issues (Kobayashi *et al.* (2019)). To resolve such problematics, NH<sub>3</sub> blending with H<sub>2</sub> or/and CH<sub>4</sub> has been proposed, to improve combustion efficiency and diminish environmental impact, which is the purpose of this work.

Studies of NH<sub>3</sub> flame enhancement by fuel addition has gained considerable attention over the last decade, although studies remain limited, with comprehensive reviews of ammonia related work undertaken (Kobayashi *et al.* (2019); Chai *et al.* (2021); Chiong *et al.* (2021)). However, further work is required to fully characterise the use of these blends. Hence, the present

work attempts to fill some outstanding gaps in the matter. The work presented herein is structured in three parts. First, the influence of the addition of H<sub>2</sub> and CH<sub>4</sub> on NH<sub>3</sub> flame reactivity is experimentally evaluated using spherically expanding flames, to measure laminar burning velocities. The resulting work can be used for numerical modelling assessments. Therefore, the second part presents results of a spherically expanding turbulent 3-D H<sub>2</sub>/NH<sub>3</sub> flame kernel using DNS, at various equivalence ratios ( $\Phi$ ). Finally, all contributions should enable practical application for design of new burner units that employ these blends. Thus, an industrial scale tangential swirl burner (8 kW) was employed and chemiluminescence traces of various species of interest (OH\*, CH\*, NH\*, NH<sub>2</sub>\*) are presented in conjunction with exhaust emissions, denoting the complexity of the use of ammonia-blends combustion.

Fundamental combustion properties of premixed NH<sub>3</sub>/air mixtures have been conducted by Hayakawa *et al.* (2015), experimentally investigating the laminar burning velocity at both atmospheric and elevated pressures, demonstrating that laminar burning velocity of NH<sub>3</sub> decreases with increasing pressure. Ichikawa *et al.* (2015) also studied the effect of pressure on the laminar flame speed and Markstein length of NH<sub>3</sub>/air flames. Their experimental studies showed that at higher pressures, the O/H radical pools are reduced, leading to decrease in flame speed as well as NO (HAYAKAWA *et al.* (2015)). Blends of CH<sub>4</sub>/NH<sub>3</sub> have been investigated by several authors (Okafor *et al.* (2018), (2019); Shu *et al.* (2021)), demonstrating a linear relationship between CH<sub>4</sub> addition and NH<sub>3</sub>/CH<sub>4</sub> flame speed. velocities Okafor *et al.* (2018) conducted experimental and numerical studies of the laminar burning velocities. A detailed reaction mechanism based on the GRI 3.0 and the mechanism by Tian *et al.* (2009) was then developed. Lee *et al.* (2010) studied experimentally and numerically the unstretched laminar flame speeds and the flame stretch response of premixed H<sub>2</sub>/NH<sub>3</sub>/air flames. The study found that at fuel rich conditions, the flame speed is significantly reduced with increasing flame stretch and in fuel lean conditions the opposite behaviour is observed. As for unstretched laminar flame speed, significant increase was observed with addition of H<sub>2</sub>. The study also found that NO<sub>x</sub> and N<sub>2</sub>O emissions increased with addition of H<sub>2</sub>, however for fuel rich conditions, the extend of increase was much lower compared to fuel lean conditions. This is because at rich conditions, NH<sub>i</sub> + NH<sub>i</sub> (where i is 1, 2) combination reactions dominate the kinetics, providing a route for NH<sub>i</sub> conversion to N<sub>2</sub> without involving NO (Dean, Chou and Stern (1984)).

Combination of CH<sub>4</sub> and NH<sub>3</sub> at lean conditions yielded low CO<sub>2</sub> emissions with the penalty of high NO<sub>x</sub> (Sullivan *et al.* (2002); Sorrentino *et al.* (2019)), while rich conditions reduced NO<sub>x</sub> emissions at the expense of producing more CO (Hewlett *et al.* (2019)). NH<sub>3</sub>/H<sub>2</sub> blends at different volumetric concentrations were studied to recognise the 80/20 and 70/30 vol. % blends as the most stable (Valera-Medina *et al.* (2019)) with low NO<sub>x</sub>

production at high equivalence ratios close to 1.2. To the authors best knowledge, CH<sub>4</sub>/NH<sub>3</sub>/H<sub>2</sub> as tertiary blends at different volumetric percentages and at  $\Phi = 1.2$  are reported here for the first time.

## PART I: LAMINAR FLAME SPEED MEASUREMENTS

### Experimental Specifications & Set-Up

Laminar flame speed measurements were performed using a constant-volume spherical vessel. Details of the rig and post-processing technique are described by Sullivan *et al.* (2002) and Sorrentino *et al.* (2019), and thus only a summary is presented here. The spherical vessel has a nominal internal volume of 4.2 L (ID 200mm), with four orthogonal 70 mm quartz viewing windows with PID temperature control. High-speed Schlieren imaging of flame propagation was achieved using a CMOS high speed camera (PHANTOM V1210 ( $\pm 0.05\%$ )) set to a suitable fast frame capture rate (5000-10000 fps) and facilitating a spatial resolution of  $\sim 0.1$  mm per pixel. Flame propagation rates were calculated by edge-detection algorithms written into a bespoke MATLAB script. Reactants were introduced into the chamber using batched thermal mass flow controllers (Brooks 5850S ( $\pm 1\%$ ), USA). Mass fractions were calculated as a function of initial pressure (P), fuel-air equivalence ratio ( $\Phi$ ), and temperature (T), with mixture concentrations confirmed by partial pressure. Internal fans were used to pre-mix the reactants, and capacitor-discharge ignition was achieved via fine electrodes mounted to  $45^\circ$  to the measurement plane. Experiments were triggered by a simultaneous TTL signal to the ignition system and data acquisition systems after quiescence had been attained. High-purity fuel components of CH<sub>4</sub> (>99.995%), H<sub>2</sub> (>99.95%), NH<sub>3</sub> (99.95%) and dry-zero grade compressed air (AirLiquide, 20.9% O<sub>2</sub>) were used to perform the experiments. Measurements were performed at initial conditions of 298 K ( $\pm 3$ K) and 0.1MPa ( $\pm 1 \times 10^{-3}$ Mpa). To investigate the influence of H<sub>2</sub> and CH<sub>4</sub> on NH<sub>3</sub> flame propagation, molar ratios were varied (0-60%, vol.), at  $\Phi=0.8, 1.0, 1.2$ , to provide a comparison of the change in flame speed with each of the binary blends. To minimize the influence of spark and pressure effects, a flame radius range of 7 to 20 mm was employed, satisfying analysis proposed by Burke *et al.* (2009) and Chen (2015). For an outwardly propagating spherical flame, the stretched flame speed ( $S_n$ ) is expressed as the temporal derivative of the Schlieren flame radius. A quasi-steady non-linear association between  $S_n$  and stretch, as proposed by Kelley and Law (2009) was utilized to obtain an extrapolated unstretched flame speed ( $S_u$ ). Burned gas expansion is then accounted for to obtain representative values of laminar burning velocities ( $S_L$ ).

### Results and Discussion

Fig. 1 presents the measured laminar burning velocities of the tested binary blends ([a]  $\Phi=0.8$ , [b]  $\Phi=1.0$ , [c]  $\Phi=1.2$ ) alongside values attained numerically. Okafor *et al.* (2019), Shrestha *et al.* (2018), and Stagni *et al.* (2020)

reaction mechanisms were appraised for H<sub>2</sub>/NH<sub>3</sub> mixtures, whilst Okafor *et al.* and Shrestha *et al.* reaction mechanisms were also evaluated for CH<sub>4</sub>/NH<sub>3</sub> blends, using the CHEMKIN-PRO PREMIX package. Note that unless otherwise stated, error bars represent maximum and minimum recorded values, around an average plotted value (minimum of 5 repeats) for laminar burning velocity values. Furthermore, it should be highlighted that due to the high minimum activation energy of NH<sub>3</sub> coupled with its very slow flame burning velocity, which results in important buoyancy effects, and thus inducing incorrect flame speeds, no experimental data is presented for 10/90 vol.% and 20/80 vol. % CH<sub>4</sub>/NH<sub>3</sub> blends at  $\Phi = 1.2$ .

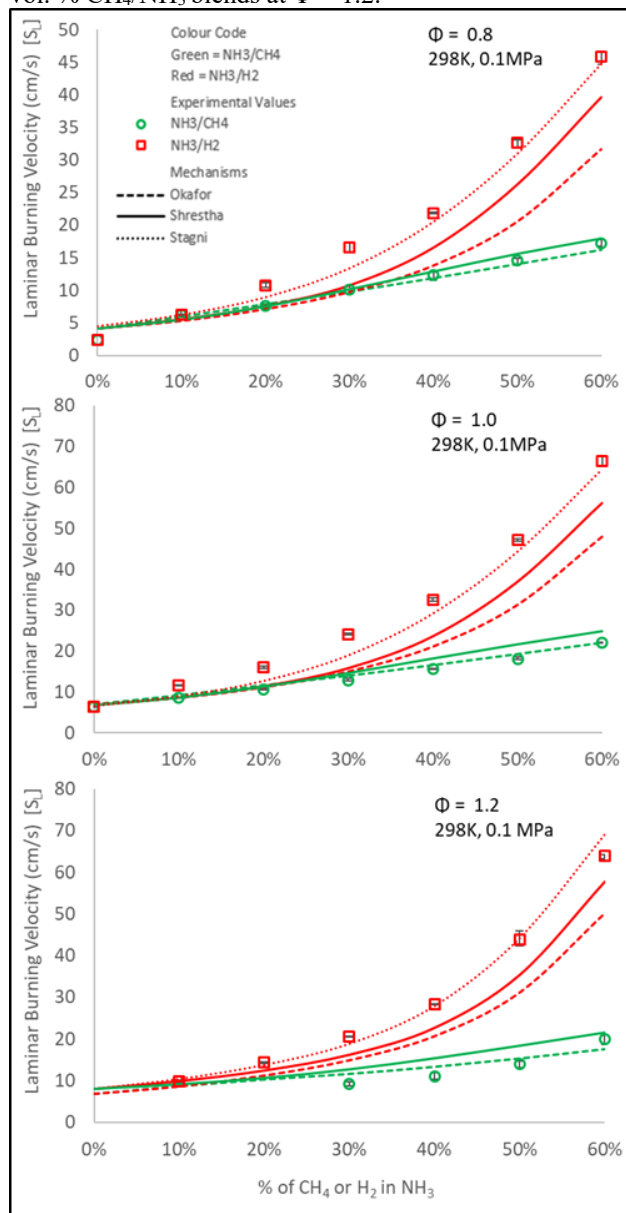


Figure 1 – Comparison of  $U_L$  for selected binary blends of NH<sub>3</sub>/CH<sub>4</sub> and NH<sub>3</sub>/H<sub>2</sub> at three equivalence ratios (a)  $\Phi = 0.8$ , (b)  $\Phi = 1.0$ , (c)  $\Phi = 1.2$  and modelled results

It is clearly observable from Fig. 1 that up to ~20% enrichment of either H<sub>2</sub> or CH<sub>4</sub> results in a similar enhancement of flame reactivity at  $\Phi = 0.8$  and 1.0. This trend is captured by the Shrestha et al. and Okafor et al. mechanism, but with significant differences only arising upon 40% enrichment of either H<sub>2</sub> or CH<sub>4</sub>. Both mechanisms, however, demonstrate very good agreement with experimental flame speeds for CH<sub>4</sub>/NH<sub>3</sub>, up to 60% CH<sub>4</sub> addition. With respect to H<sub>2</sub>/NH<sub>3</sub> binary blends, excellent agreement is displayed with the Stagni mechanism, with less good agreement is exhibited by the Shrestha et al. mechanism, which under-predicts the influence of H<sub>2</sub> on NH<sub>3</sub> flame speed above 10% H<sub>2</sub> addition, irrespective of the  $\Phi$ . The Okafor mechanism seems unsuitable for modelling H<sub>2</sub>/NH<sub>3</sub> mixtures, greatly underpredicting flame speeds at all conditions studied. Overall, a linear correlation between added molar CH<sub>4</sub> fraction and flame speed of CH<sub>4</sub>/NH<sub>3</sub> is clearly identifiable, observed both experimentally and numerically, at all tested conditions. This same linear relation is also observed up to 20% H<sub>2</sub> enrichment in NH<sub>3</sub>, prior to an exponential increase in flame speed upon further H<sub>2</sub> addition.

To better understand these changes in flame response, modelling of freely propagating flames was undertaken, using the CHEMKIN-PRO software package. The computational solutions were based on an adaptive grid of 1000 points, including multi-component diffusion and an assumed air composition of 79% N<sub>2</sub> – 21% O<sub>2</sub>. The Stagni and Okafor mechanisms were utilized for H<sub>2</sub>/NH<sub>3</sub> and CH<sub>4</sub>/NH<sub>3</sub>, respectively, since they displayed the best agreement with experimental measurements. The aforementioned mechanisms were employed to generate numerical adiabatic flame temperatures ( $T_{ad}$ ), volumetric heat release rates ( $Q'$ ) and concentration of mole fractions of active radicals (H and O). Modelled increases in  $T_{ad}$  upon H<sub>2</sub> and CH<sub>4</sub> addition to NH<sub>3</sub> were observed to be comparable (at  $\Phi = 1.0$ , 60% addition of H<sub>2</sub> and CH<sub>4</sub> resulted in an increase in  $T_{ad}$  of  $\approx 129$  K and 113 K, respectively: with H<sub>2</sub> enhancing  $T_{ad}$  to a greater extent than CH<sub>4</sub> at lean and rich conditions). However, modelling work predicts a significant augmentation of burning intensity (through the volumetric heat release rate,  $Q'$ ), due to the presence of H<sub>2</sub> than CH<sub>4</sub>, with relative increases in  $Q'$ , normalized to that of pure NH<sub>3</sub>, presented in Figure 2 ([a]  $\Phi=0.8$ , [b]  $\Phi=1.0$ , [c]  $\Phi=1.2$ ). Note, however, that the heat of combustion per mass (KJ/mol) of H<sub>2</sub> is ~4 times greater than that of CH<sub>4</sub> (H<sub>2</sub>  $\approx 286$ ; CH<sub>4</sub>  $\approx 74$  [KJ/mol]), however, it is noted that there are significant differences in terms of molecular mass between both fuels (H<sub>2</sub>  $\approx 2$ ; CH<sub>4</sub>  $\approx 16$  [g/mol]).

Evidently, relative increases in  $Q'$  for CH<sub>4</sub>/NH<sub>3</sub> and H<sub>2</sub>/NH<sub>3</sub> blends exhibit the same linear and exponential trend as observed for the laminar flame speeds. Interestingly, modelled values predict that up to 20% addition of either H<sub>2</sub> or CH<sub>4</sub> result in comparable relative increases in  $Q'$ , analogous to the similar measured flame speeds. Augmented volumetric heat release rates result in

enhanced production of key radicals, notably H and O, with modelled values of relative increases in H and O radical production superimposed in Fig. 2. Again, the relative increases in the production of H and O radicals exhibit the same linear and exponential trends to that displayed by changes in measured flame speed and modelled  $Q'$ , for CH<sub>4</sub>/NH<sub>3</sub> and H<sub>2</sub>/NH<sub>3</sub> blends, respectively, with divergence only arising at 20% additions of H<sub>2</sub> and CH<sub>4</sub> to NH<sub>3</sub>. Consequently, it seems that the measured enhancement of NH<sub>3</sub> with CH<sub>4</sub> or H<sub>2</sub> may not primarily be a thermal effect (since modelling changes in  $T_{ad}$  are similar) but potentially a diffusional or kinetic effect.

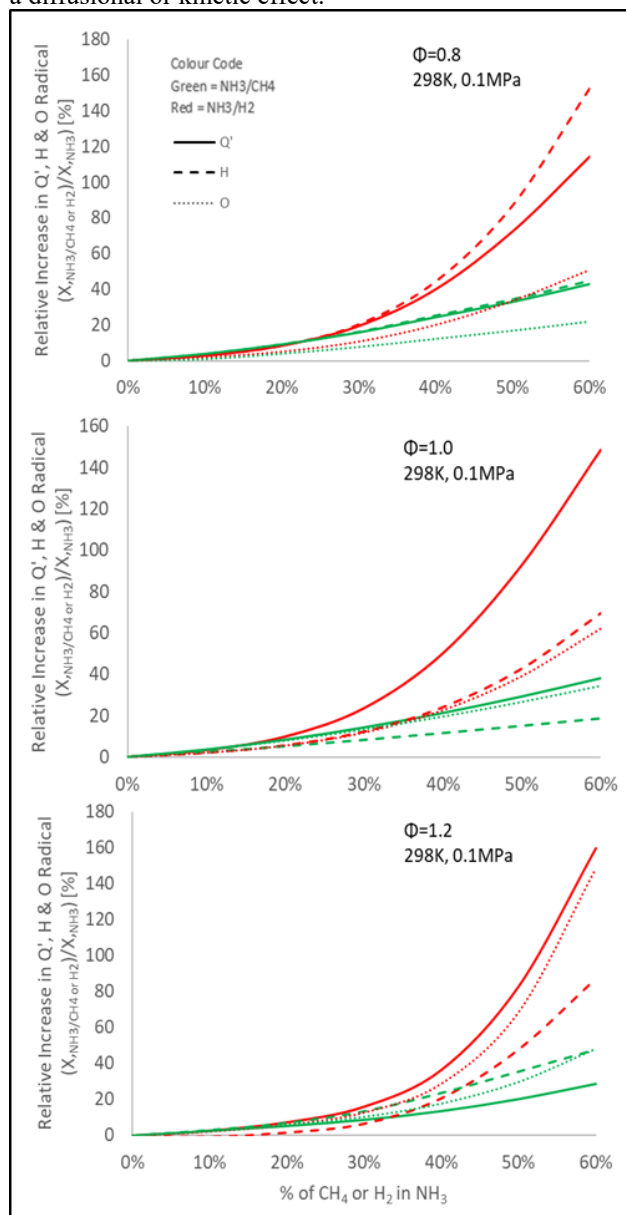


**Figure 2 – Relative Increase in Modelled volumetric heat release rate  $Q'$ , H and O Radical Production for CH<sub>4</sub>/NH<sub>3</sub> and H<sub>2</sub>/NH<sub>3</sub> Mixtures (a)  $\Phi = 0.8$ , (b)  $\Phi = 1.0$ , (c)  $\Phi = 1.2$  (Note: Modelled Results divided by a factor of 20)**

**Table 1 – Relative Change in activation energy ( $E_a$ ) upon  $H_2$  and  $CH_4$  addition to  $NH_3$  ( $E_a$  for  $H_2/NH_3$  and  $CH_4/NH_3$  modelled using Stagni and Okafor Mechanisms, respectively).**

% Vol.	Relative Change in $NH_3$ Activation Energy (%)					
	$H_2$			$CH_4$		
	$\Phi$			$\Phi$		
$H_2$ or $CH_4$	0.8	1.0	1.2	0.8	1.0	1.2
10%	-2.4	-5.7	-4.2	-8.2	-5.4	-0.3
20%	-10.0	-9.8	-12.4	-11.6	-7.0	-1.0
30%	-29.6	-21.0	-11.4	-15.9	-10.3	-0.4
40%	-34.4	-20.0	-13.3	-17.8	-13.7	+0.2
50%	-37.8	-27.6	-15.2	-25.3	-13.5	+2.0
60%	-43.5	-34.2	-24.2	-24.3	-19.4	-3.7

From the measured and modelled results, up to 20%  $CH_4$  or  $H_2$  addition affects the overall oxidation mechanics of  $NH_3$  in a similar manner, prior to enhanced reactivity being displayed upon further  $H_2$  addition, reflected in substantially augmented flame speeds. The minimum activation energy ( $E_a$ ) of the tested blends was numerically modelled, evaluated using the Müller, Bollig and Peters (1997) approximation and the flame temperature profile generated using the ChemKin Pro software. The Stagni and Okafor mechanisms were utilized for  $H_2/NH_3$  and  $CH_4/NH_3$  mixtures, respectively. Relative changes in  $E_a$  of  $NH_3$  due to the presence of either  $H_2$  or  $CH_4$ , normalized to that of pure  $NH_3$ , are represented in Table 3 (with a ‘-’ and ‘+’ sign representing a relative decrease or increase, respectively, in minimum activation energy). Unsurprisingly, since the activation energy of  $H_2$  is approximately at least half of that of  $CH_4$  ( $E_a H_2 \approx 25$  kcal/mol,  $E_a CH_4 \approx 50$  kcal/mol at  $\Phi=1.0$ ), a greater reduction in  $E_a$  of  $NH_3$  is expected with the presence of  $H_2$ , which the case for all evaluated blends. Of interest, however, is that up to 20% addition of  $CH_4$  or  $H_2$ , result in quasi-identical reductions in  $E_a$  at  $\Phi = 0.8$  and  $1.0$  ( $\Phi=0.8$ ; a relative decrease of 10% [ $H_2$ ] and 11.6% [ $CH_4$ ];  $\Phi = 1.0$  a relative decrease of 9.8% [ $H_2$ ] and 7.0% [ $CH_4$ ]). This is in good agreement with both modelled average relative increases in  $Q'$ ,  $H$  and  $O$  radical production, as well as similar changes in measured laminar burning velocities. Above 20% volumetric additions,  $H_2$  substitution results in nearly 1.5 to 2 times greater reduction in  $E_a$  than an equivalent  $CH_4$  addition to  $NH_3$ , at lean and stoichiometric conditions, again in good agreement with enhanced reactivity of  $H_2/NH_3$  flames compared to that of  $CH_4/NH_3$  flames above 20% addition. Interestingly, at rich conditions ( $\Phi=1.2$ ), whilst  $H_2$  addition still significantly reduces the  $E_a$  of  $NH_3$ , equal  $CH_4$  addition seems to yield very little change (reduction of only 3.7% at 60%  $CH_4$  addition). As such, changes in flame speed in rich  $CH_4/NH_3$  mixtures, may potentially be less influenced by kinetic effects, but rather thermal (greatest change in  $T_{ad}$  was evaluated at  $\Phi=1.2$ ) or diffusional pathways play a more important role. However, to elucidate the precise nature of augmented laminar flame speeds of rich  $CH_4/NH_3$  blends, a more elaborate sensitivity study would have to be conducted. These results can be used for validation of bespoke numerical models, described next.

## PART II: NUMERICAL STUDIES OF $NH_3/H_2/AIR$ FLAME KERNELS USING DNS

Several studies of ammonia flames in turbulent conditions have been carried out as well. Ichimura et al. studied the extinction limits of  $NH_3$  flames propagating in a turbulent environment (Ichimura *et al.* (2019)). The study showed that for  $NH_3/air$  flames, the highest turbulence intensity was reached for an equivalence ratio of  $\Phi=0.9$  even though the maximum laminar burning velocity was for  $\Phi=1.1$ . Netzer *et al.* (2021) studied the effect of curvature on the production of  $NO$  in  $NH_3/H_2/air$  flames. It was observed that in globally lean flames, local increase in equivalence ratio, due to preferential diffusion leads to increase in  $NO$  formation, while for globally rich flames, the opposite effect is observed. Mikulčić *et al.* (2021) studied various reaction mechanisms for gas turbine applications and found that the San Diego mechanism was very capable in prediction of emissions, however none of the studied mechanisms were able to accurately predict  $CO$  emissions.

### Numerical Set-Up and Conditions

DNS studies of spherically expanding turbulent 3-D flame kernels were conducted. The DNS cases were run using an in-house finite difference code. The code uses Lele’s 6th order compact differencing scheme (Lele (1992)) and De Lange’s 5th order upwind scheme (Lange (2005)) for the convective terms to avoid numerical diffusion. The time discretization was done using a 3rd order compact Runge-Kutta scheme (Kennedy, Carpenter and Lewis (2000)). The boundary conditions were modelled using the Navier=Stokes characteristic boundary conditions (Poinsot and Lele (1992)). Subsonic outflow conditions were imposed for all faces of the cubic domain of  $15mm \times 15mm \times 15mm$  used for this study.

Following a mesh dependency study, the grid size for these simulations were chosen in such a way that there are always 14 or more cells for the laminar flame thickness which ensures that the solution is independent of the mesh size. A time step of  $1e-8s$  was used for all the cases, as this ensures stability of the code. The initial turbulence was generated by convoluting a random stream function with a filter. The gradient of the resulting field produces the velocity field. This way the turbulence is homogenous, isotropic and divergence free (by definition). The integral length scale can be selected by choosing a particular filter width. The chemistry was initialized by converting a 1D flame, generated using CHEM1D (Somers (1994)) into a 3D flame kernel. The cases studied in this paper are detailed in. The cases were selected to compare three equivalence ratios of 0.8, 1 and 1,2 of 50%  $H_2$  and 50%  $NH_3$  combustion in air at constant  $Ka$  of 10, and  $\frac{l_t}{l_f}$  of 1, where  $Ka$  is the Karlowitz number,  $l_t$  the integral length scale and  $l_f$  the laminar flame length. Diffusion is modelled using the constant Lewis approach, where the Lewis numbers are obtained from a 1D

adiabatic flame solution computed using a multi-component diffusion model including thermal diffusion.

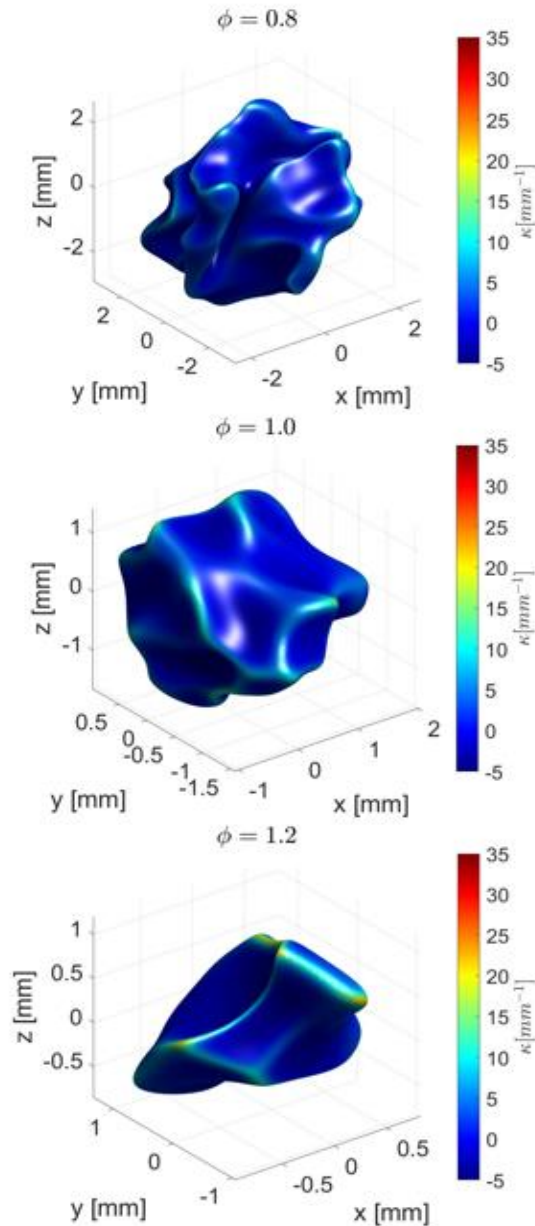


**Figure 3: Flame structure taken at temperature iso-levels of the laminar inner layer temperature after 1 eddy turnover time at different equivalence ratios.**

### Results and Discussion

The flame structure after one eddy turnover time is shown in Fig.3. Clearly, the lean flame kernel is wrinkled on a smaller scale than compared to the stoichiometric and rich case. Particularly interesting is the smooth flame surface of the rich case, with strongly curved leading edges. This can be explained by looking at the conditional mean of

the heat release rate, scaled to the minimum and maximum of the corresponding stretchless 1D flamelets.

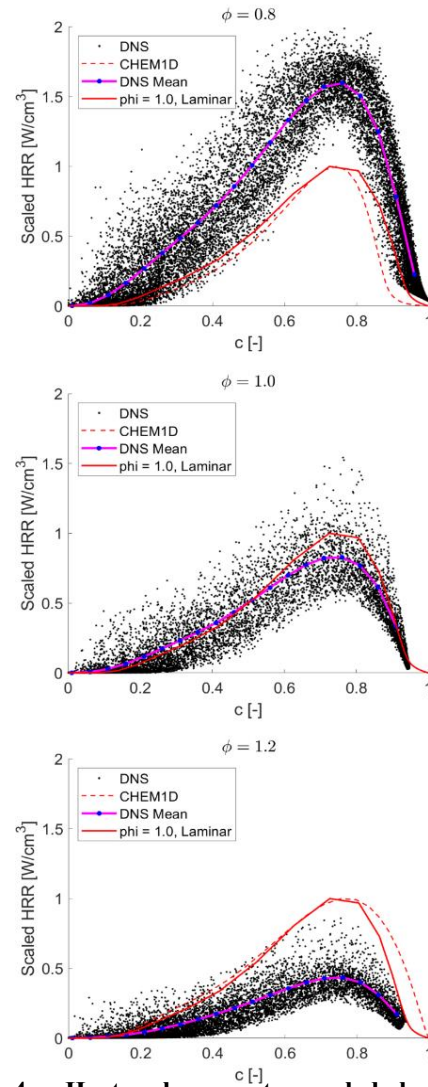


**Figure 4: Heat release rate, scaled by limits of corresponding 1D unstrained flames, with respect to the progress variable. Significant deviation from 1D flame behaviour seen for rich mixture.**

In Fig.4 the mean heat release rate, conditioned at the progress variable, scaled to the minimum and maximum of the corresponding stretch less 1D flamelets have been plotted. We can see that the heat release rate decreases with equivalence ratio compared to the 1D solutions. For the lean case, the turbulence interacts with the chemistry, increasing the reaction rate significantly. The stoichiometric case is quite close to the unstretched laminar 1D behaviour and finally very high difference from laminar behaviour is seen for the rich case. This was also observed by Lee *et al.* (2010), where for fuel rich conditions the flame speed, and consequently the heat release, significantly reduced on applying stretch while the opposite behaviour was observed for lean cases.

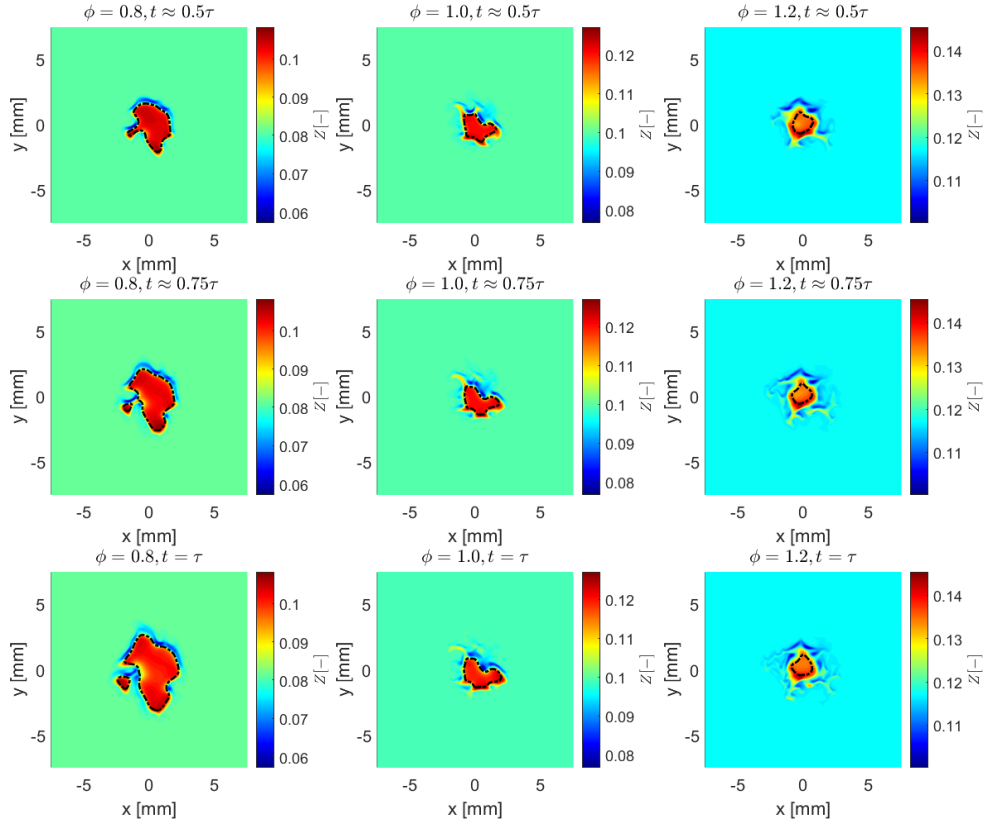


**Figure 5: Mixture fraction values for all three cases at 0.5, 0.75 and 1 times the eddy turnover time,  $\tau$  taken at mid-plane along the  $z$  axis. The dash-dot lines indicate the laminar inner layer temperature.**

In Fig.5 snapshots of the flame at the mid-plane along the  $z$  axis at different time steps are plotted. It is observed that as the equivalence ratio increases, the turbulence affects mixture composition at the flame front significantly and is more sensitive to curvature effects. This was also observed in rich ammonia/methane flames by Okafor *et al.* (2018). For the rich case, large disturbances due to the turbulence can be seen as well. Since the constant  $Ka$  ensures that the chemical time scale is 0.1 times the Kolmogorov time scale, we can conclude that the small-scale turbulent structures affect the flame chemistry in such a way that it suppresses the combustion chemistry in turbulent spherically expanding flame kernels.

Results obtained from the development of these models will enable better resolution of more complex, larger models, such as those intended for industrial scale systems fuelled with  $NH_3/H_2/CH_4$  blends similar to the one presented next.

### PART III: TANGENTIAL SWIRL BURNER

An industrial-scale tangential swirl burner was employed with a constant thermal power of 10 kW, equivalence ratio,  $\Phi = 1.2$  and a swirl no. ( $S_g$ ) of 1.05. A set of Bronkhorst mass flow controllers (MFCs) was used to regulate the fuel and air flows with a precision of  $\pm 0.5\%$ .

Fig. 6 shows the schematic of the tangential burner. Methane and ammonia were fully premixed with air flow, whereas hydrogen flows were introduced 4 cm below the burner exit, directly into the swirler through 6 equispaced injection holes with 1.5mm diameter, angled at  $45^\circ$  for better mixing with the rest of the mixtures prior to ignition. A quartz tube made from GE214 material (*GE 124/214 Quartz | Specialty Glass Products (2019)*) was used for optical diagnostics. All the experiments were conducted at ambient inlet pressure and temperature. A pair of LaVision CCD cameras with UV and visible ranges were employed to obtain chemiluminescence traces of various species of interest. The units were triggered simultaneously with 90% gain and a gate-time of 700,000 ns. Various Edmund filters were used for each species, namely  $OH^*$  (310 nm),  $CH^*$  (420 nm),  $NH^*$  (337 nm),  $NH_2^*$  (630 nm). LaVision Davis v10 was used to gather 200 frames per experimental points, which were then post-processed using a be-spoke MATLAB script (Mashruk (2020)) designed to conduct Abel Inversion after averaging.

Exhaust emissions were sampled and measured using Emerson CT5100 Continuous Quantum Cascade Laser analyser at a frequency of 1 Hz with a repeatability of  $\pm 1\%$  and 0.999 linearity. Sampling temperatures were maintained at 433K to avoid condensation.

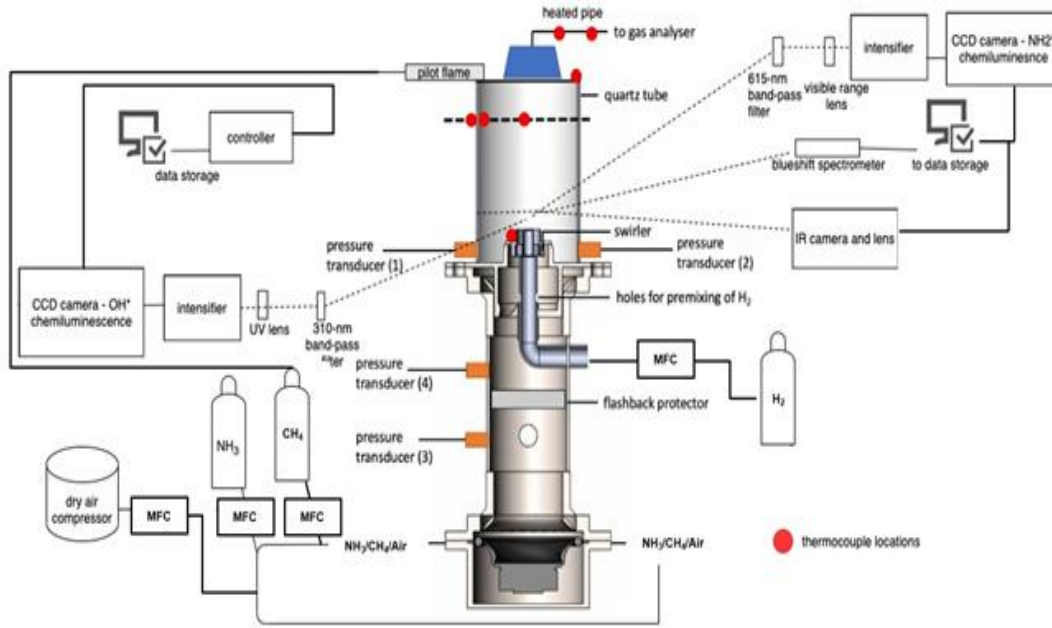
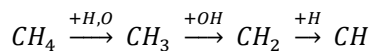


**Figure 6: Schematic of tangential swirl combustor with measuring techniques and control systems.**

## Results and Discussion

Fig. 7 displays the experimental points undertaken in the tangential swirl burner, as well as the formation of species of interest. Colourmaps were normalised to species dataset maximum to observe the changes in species formation with varying fuel blend composition. OH\*, CH\* and NH\* formation decreases with decreasing CH<sub>4</sub> and increasing NH<sub>3</sub> mol fraction, whereas NH<sub>2</sub>\* displays opposite trend. There are definitive changes in the flame shapes and thicknesses with NH<sub>3</sub> vol.% ≥ 50%.

OH radicals play an important role to oxidise the fuel and reduce ignition delay time in hydrogen based fuels (Warnatz, Maas and Dibble (2006); Mashruk, Xiao and Valera-Medina (2020)). The major source of OH radicals is from the reaction between H radicals and O<sub>2</sub> molecules. However, H radicals are mainly produced from CH<sub>4</sub> reacting with third body elements. Thus, OH formation decreases with decreasing CH<sub>4</sub> content in the fuel. The production of CH\* is directly correlated to the CH<sub>4</sub> content in the fuel, as expected. CH radical production follows the below path from CH<sub>4</sub>.



NH\* was observed in high concentration at high methane content blends, a trend that decayed into higher NH<sub>2</sub>\* patterns at high ammonia content blends. The major source of NH in the flame are from HCN through reaction R1 but HCN is largely produced from the CH radicals, reacting with NO and molecular nitrogen. The only source

of amidogen (NH<sub>2</sub>) production is from ammonia reacting with H radicals (reaction R2) and third body elements (reaction R3). It must be noted that reaction R3 has very minor contribution compared to reaction R2. Thus, NH<sub>2</sub>\* intensity increases with increasing NH<sub>3</sub> content in the blends, Fig. 7.

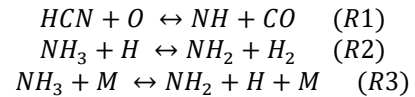
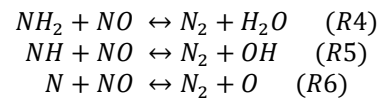
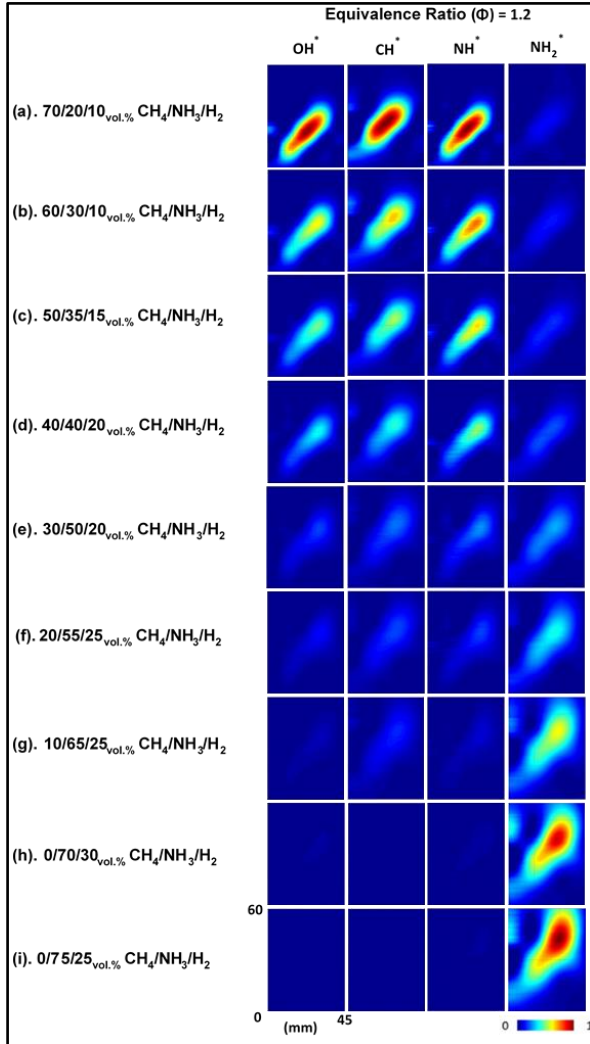


Fig. 8 shows the 15% O<sub>2</sub>, dry NO<sub>x</sub> and unburnt NH<sub>3</sub> emissions at varying fuel blends, Fig. 7, measured at the exhaust. It must be noted that red markers in Fig. 8 represents greater than value, rather than exact measured emissions, as the emitted values were out of the gas analyser measurement ranges at those points. NO emissions decrease significantly with increasing ammonia content in the fuel blend, indicating NO productions from thermal and prompt pathways at the presence of methane in the blend. At the rich condition with ammonia content more than 50% considered here, NO emissions decrease considerably due to the conversion to N<sub>2</sub> through the reactions R4, R5 and R6.



Ammonia emissions at exhaust follows an interesting trend with increasing ammonia and decreasing methane content in the blends, Fig. 8. Ammonia emissions increases

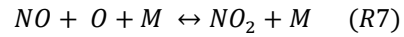
with increasing ammonia content up to 40%, then decreases with ammonia content between 50-55%, followed by significant increase above 55% ammonia content.



**Figure 7.** Abel transformed  $\text{OH}^*$ ,  $\text{CH}^*$ ,  $\text{NH}^*$  and  $\text{NH}_2^*$  chemiluminescence for the experimental points in tangential swirl burner. Colourmap normalised to species dataset max.

In the presence of high temperature and excess H radicals (from methane) and third body elements at the post-flame zone, reaction R3 operates backwards to produce  $\text{NH}_3$  from  $\text{NH}_2$ , thus increased ammonia emissions up to 40%  $\text{NH}_3$  in the blend. However, as the H radicals production decreases with decreasing methane content, as well as with decreasing flame temperature, reaction R3 cannot achieve minimum activation energy to operate backwards, thus giving low ammonia emissions at 50 and 55% ammonia blends. At 65% and above ammonia blends considered here, there are not enough methane in the flame to produce enough H radicals to burn all the  $\text{NH}_3$  contents in the fuel, giving high unburnt ammonia emissions.

$\text{NO}_2$  and  $\text{N}_2\text{O}$  emissions are quite low compared to  $\text{NO}$  and  $\text{NH}_3$  emissions for the fuel blends considered here. At the presence of high methane content in the blends,  $\text{NO}$  converts to  $\text{NO}_2$  and vice-versa through the reactions R7 and R8, respectively. However, at high ammonia content blends,  $\text{NO}$  converts to  $\text{NO}_2$  by reacting with  $\text{HO}_2$  and the third body reaction R7.



$\text{N}_2\text{O}$ , a GHG that is known to possess up to 300 times the Global Warming Potential (GWP) of  $\text{CO}_2$  (Houghton, Jenkins and Ephraums no date) seems to have very low emissions at the fuel blends considered here at rich condition. The major source of  $\text{N}_2\text{O}$  emissions in high ammonia fuel content is through reaction R9, which interestingly operate backwards at the presence of high methane content in the fuel to produce  $\text{NO}$ . Reaction R10 is responsible for  $\text{N}_2\text{O}$  production at the presence of high methane content. At both scenarios,  $\text{N}_2\text{O}$  reacts with H radicals to convert to  $\text{N}_2$  and OH radicals. It must be noted that  $\text{CO}_2$  emissions were over 10% for all the  $\text{CH}_4$  blends considered here at  $\Phi = 1.2$ , as expected.

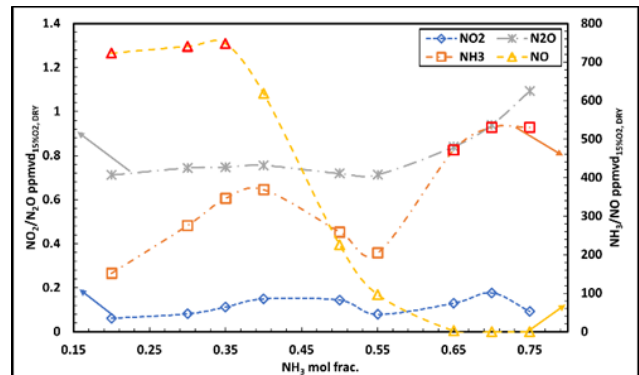
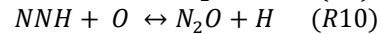
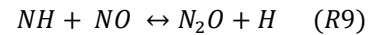


**Figure 8.** Measured emissions at the exhaust. Red markers indicate greater than values.

## CONCLUSIONS

Blends of  $\text{H}_2/\text{NH}_3$  and  $\text{CH}_4/\text{NH}_3$  have been investigated using a variety of techniques to holistically approach the resolution of ammonia-blends combustion, enabling a better understanding of these molecules for fundamental and applied purposes. Initially, the work employed a spherically expanding flame configuration to measure flame speeds. Secondly, DNS modelling of  $\text{H}_2/\text{NH}_3$  (50%/50%) across lean to rich conditions has been presented. Finally, chemiluminescence of important species and measured emissions of tertiary blends of  $\text{H}_2/\text{CH}_4/\text{NH}_3$  have been examined using an industrial-scale tangential swirl burner. From these works the following can be concluded:

(1). The laminar burning velocity of NH<sub>3</sub> increases linearly with CH<sub>4</sub> addition, with the Shrestha et al. and Okafor displaying very good agreement with measured results. An exponential increase in flame speed of NH<sub>3</sub> is observed with increasing H<sub>2</sub> addition, with the Stagni mechanism exhibiting excellent agreement, with other investigated reaction mechanisms underpredicting the influence of H<sub>2</sub> on NH<sub>3</sub> flame reactivity.

(2). Equal volumetric additions of CH<sub>4</sub> and H<sub>2</sub> up to 20% equate to a similar enhancement of NH<sub>3</sub> reactivity across all tested equivalence ratios. Modelling work suggests that increases in flame speed, burning intensity and O and H radical concentrations are highly correlated in agreement with literature. Measured augmentations of flame speed of lean and stoichiometric CH<sub>4</sub>/NH<sub>3</sub> and H<sub>2</sub>/NH<sub>3</sub> blends seem to be principally an Arrhenius effect, through the reduction of the global activation energy.

(3). Modelled lean 50% hydrogen 50% ammonia flame kernels show small scale flame surface wrinkling compared to the rich case. For the lean case, preferential diffusion effects due to flame curvature pushes local equivalence ratio to near stoichiometric values, thereby increasing the heat release rate. The opposite effect is observed for rich case, where due to the further increase in local equivalence ratio, the heat release rate is reduced.

(4). CH<sub>4</sub> is found to be the main source of OH\* and CH\*, while NH<sub>2</sub>\* is mainly produced from NH<sub>3</sub>. NO production decreases with increasing NH<sub>3</sub> concentrations, while unburned ammonia emissions increase considerably at high NH<sub>3</sub> blends. NO<sub>2</sub> and N<sub>2</sub>O emissions are found to be very low at the blends and power considered here.

#### ACKNOWLEDGEMENT

This project has received funding from the European Union's Horizon 2020 research and innovation programme under grant agreement No 884157.

#### REFERENCES

Burke, M.P. *et al.* (2009) 'Effect of cylindrical confinement on the determination of laminar flame speeds using outwardly propagating flames', *Combustion and Flame*, 156(4), pp. 771–779. doi:10.1016/j.combustflame.2009.01.013.

Chai, W.S. *et al.* (2021) 'A review on ammonia, ammonia-hydrogen and ammonia-methane fuels', *Renewable and Sustainable Energy Reviews*, 147(May), p. 111254. doi:10.1016/j.rser.2021.111254.

Chen, J., Fei, Y. and Wan, Z. (2019) 'The relationship between the development of global maritime fleets and GHG emission from shipping', *Journal of Environmental Management*, 242(April), pp. 31–39. doi:10.1016/j.jenvman.2019.03.136.

Chen, Z. (2015) 'On the accuracy of laminar flame speeds measured from outwardly propagating spherical flames: Methane/air at normal temperature and pressure', *Combustion and Flame*, 162(6), pp. 2442–2453. doi:10.1016/j.combustflame.2015.02.012.

Chiong, M.C. *et al.* (2021) 'Advancements of combustion technologies in the ammonia-fuelled engines', *Energy Conversion and Management*, 244(June), p. 114460. doi:10.1016/j.enconman.2021.114460.

Dean, A.M., Chou, M. -S and Stern, D. (1984) 'Kinetics of rich ammonia flames', *International Journal of Chemical Kinetics*, 16(6), pp. 633–653. doi:10.1002/kin.550160603.

GE 124/214 Quartz | Specialty Glass Products (2019). Available at: <https://www.sgpinc.com/materials/fused-quartz/ge-124214-quartz/> (Accessed: 28 July 2021).

Hayakawa, A. *et al.* (2015) 'Laminar burning velocity and Markstein length of ammonia/air premixed flames at various pressures', *Fuel*, 159, pp. 98–106. doi:10.1016/j.fuel.2015.06.070.

HAYAKAWA, A. *et al.* (2015) 'NO formation/reduction mechanisms of ammonia/air premixed flames at various equivalence ratios and pressures', *Mechanical Engineering Journal*, 2(1), pp. 14-00402-14-00402. doi:10.1299/mej.14-00402.

Hewlett, S.G. *et al.* (2019) 'Gas turbine co-firing of steelworks ammonia with coke oven gas or methane: A fundamental and cycle analysis', in *Proceedings of the ASME Turbo Expo*. Phoenix, Arizona, pp. GT2019-91404. doi:10.1115/GT2019-91404.

Houghton, J.T., Jenkins, G.J. and Ephraums, J.J. (eds) no date *Climate Change - The IPCC Scientific Assessment*. Cambridge: Cambridge University Press. Available at: [https://www.ipcc.ch/site/assets/uploads/2018/03/ipcc\\_far\\_wg\\_I\\_full\\_report.pdf](https://www.ipcc.ch/site/assets/uploads/2018/03/ipcc_far_wg_I_full_report.pdf) (Accessed: 30 July 2021).

I.E.A (2019) *The Future of Hydrogen - Seizing today's opportunities*.

Ichikawa, A. *et al.* (2015) 'Laminar burning velocity and Markstein length of ammonia/hydrogen/air premixed flames at elevated pressures', *International Journal of Hydrogen Energy*, 40(30), pp. 9570–9578. doi:10.1016/j.ijhydene.2015.04.024.

Ichimura, R. *et al.* (2019) 'Extinction limits of an ammonia/air flame propagating in a turbulent field', *Fuel*, 246(December 2018), pp. 178–186. doi:10.1016/j.fuel.2019.02.110.

Kelley, A.P. and Law, C.K. (2009) 'Nonlinear effects in the extraction of laminar flame speeds from expanding spherical flames', *Combustion and Flame*, 156(9), pp. 1844–1851. doi:10.1016/j.combustflame.2009.04.004.

Kennedy, C.A., Carpenter, M.H. and Lewis, R.M. (2000) 'Low-storage, explicit Runge–Kutta schemes for the compressible Navier–Stokes equations', *Applied Numerical Mathematics*, 35(3), pp. 177–219. doi:10.1016/S0168-9274(99)00141-5.

Kobayashi, H. *et al.* (2019) 'Science and technology of ammonia combustion', *Proceedings of the Combustion Institute*, 37(1), pp. 109–133. doi:10.1016/j.proci.2018.09.029.

Lange, H.C. de (2005) 'Inviscid flow modelling using asymmetric implicit finite difference schemes', *International Journal for Numerical Methods in Fluids*, 49(9), pp. 1033–1051. doi:10.1002/FLD.1044.

- Lee, J.H. *et al.* (2010) ‘Studies on properties of laminar premixed hydrogen-added ammonia/air flames for hydrogen production’, *International Journal of Hydrogen Energy*, 35(3), pp. 1054–1064. doi:10.1016/j.ijhydene.2009.11.071.
- Lele, S.K. (1992) ‘Compact finite difference schemes with spectral-like resolution’, *Journal of Computational Physics*, 103(1), pp. 16–42. doi:10.1016/0021-9991(92)90324-R.
- Letcher, T. (2015) *Climate Change: Observed Impacts on Planet Earth*. 2nd edn. Elsevier.
- Mashruk, S. (2020) *NO Formation Analysis using Chemical Reactor Modelling and LIF Measurements on Industrial Swirl Flames - PhD Thesis*. Cardiff University. doi:10.13140/RG.2.2.28297.06246/1.
- Mashruk, S., Xiao, H. and Valera-Medina, A. (2020) ‘Rich-Quench-Lean model comparison for the clean use of humidified ammonia/hydrogen combustion systems’, *International Journal of Hydrogen Energy*, 46(5), pp. 4472–4484. doi:10.1016/j.ijhydene.2020.10.204.
- Mikulčić, H. *et al.* (2021) ‘Numerical simulation of ammonia/methane/air combustion using reduced chemical kinetics models’, *International Journal of Hydrogen Energy*, 46(45), pp. 23548–23563. doi:10.1016/J.IJHYDENE.2021.01.109.
- Müller, U.C., Bollig, M. and Peters, N. (1997) ‘Approximations for burning velocities and Markstein numbers for lean hydrocarbon and methanol flames’, *Combustion and Flame*, 108(3), pp. 349–356. doi:10.1016/S0010-2180(96)00110-1.
- Netzer, C. *et al.* (2021) ‘Curvature effects on NO formation in wrinkled laminar ammonia/hydrogen/nitrogen-air premixed flames’, *Combustion and Flame*, 232, p. 111520. doi:10.1016/J.COMBUSTFLAME.2021.111520.
- Okafor, E.C. *et al.* (2018) ‘Experimental and numerical study of the laminar burning velocity of CH<sub>4</sub>-NH<sub>3</sub>-air premixed flames’, *Combustion and Flame*, 187, pp. 185–198. doi:10.1016/j.combustflame.2017.09.002.
- Okafor, E.C. *et al.* (2019) ‘Measurement and modelling of the laminar burning velocity of methane-ammonia-air flames at high pressures using a reduced reaction mechanism’, *Combustion and Flame*, 204, pp. 162–175. doi:10.1016/j.combustflame.2019.03.008.
- Pivovar, B. (2016) *H<sub>2</sub> at Scale: Deeply Decarbonizing Our Energy Systems*.
- Poinsot, T.J. and Lele, S.K. (1992) ‘Boundary conditions for direct simulations of compressible viscous flows’, *Journal of Computational Physics*, 101(1), pp. 104–129. doi:10.1016/0021-9991(92)90046-2.
- Ritchie, H. and Roser, M. (2020) *Energy, Our World in Data*.
- Service, R. (2018) ‘Liquid Sunshine’, *Science*, 361(6398), pp. 120–123.
- Shrestha, K.P. *et al.* (2018) ‘Detailed Kinetic Mechanism for the Oxidation of Ammonia Including the Formation and Reduction of Nitrogen Oxides’, *Energy and Fuels*, 32(10), pp. 10202–10217. doi:10.1021/acs.energyfuels.8b01056.
- Shu, T. *et al.* (2021) ‘An experimental study of laminar ammonia / methane / air premixed flames using expanding spherical flames’, 290(September 2020).
- Somers, L.M.T. (1994) *The simulation of flat flames with detailed and reduced chemical models*. Technische Universiteit Eindhoven. doi:10.6100/IR420430.
- Sorrentino, G. *et al.* (2019) ‘Low-NO<sub>x</sub> conversion of pure ammonia in a cyclonic burner under locally diluted and preheated conditions’, *Applied Energy* [Preprint]. doi:10.1016/j.apenergy.2019.113676.
- Stagni, A. *et al.* (2020) ‘An experimental, theoretical and kinetic-modeling study of the gas-phase oxidation of ammonia’, *Reaction Chemistry and Engineering*, 5(4), pp. 696–711. doi:10.1039/c9re00429g.
- Sullivan, N. *et al.* (2002) ‘Ammonia conversion and NO<sub>x</sub> formation in laminar coflowing nonpremixed methane-air flames’, *Combustion and Flame* [Preprint]. doi:10.1016/S0010-2180(02)00413-3.
- Tian, Z. *et al.* (2009) ‘An experimental and kinetic modeling study of premixed NH<sub>3</sub>/CH<sub>4</sub>/O<sub>2</sub>/Ar flames at low pressure’, *Combustion and Flame*, 156(7), pp. 1413–1426. doi:10.1016/j.combustflame.2009.03.005.
- Valera-Medina, A. *et al.* (2019) ‘Premixed ammonia/hydrogen swirl combustion under rich fuel conditions for gas turbines operation’, *International Journal of Hydrogen Energy*, 44(16), pp. 8615–8626. doi:10.1016/j.ijhydene.2019.02.041.
- Warnatz, J., Maas, U. and Dibble, R.W. (2006) *Combustion: Physical and Chemical Fundamentals, Modeling and Simulation, Experiments, Pollutant Formation*. 4th edn. Berlin Heidelberg: Springer-Verlag. Available at: <https://www.springer.com/gp/book/9783540259923>.